# A three-level linearized time integration scheme for tumor simulations with Cahn-Hilliard equations

Maciej Smołka[1][0000−0002−3386−0555], Maciej Woźniak[1][0000−0002−5576−5671], and Robert Schaefer[1][0000−0002−1669−2086]

Institute of Computer Science
AGH University of Science and Technology, Kraków, Poland
{smolka,macwozni,schaefer}@agh.edu.pl
https://informatyka.agh.edu.pl/

**Abstract.** The paper contains an analysis of a three-level linearized time integration scheme for Cahn-Hilliard equations. We start with a rigorous mixed strong/variational formulation of the appropriate initial boundary value problem taking into account the existence and uniqueness of its solution. Next we pass to the definition of two time integration schemes: the Crank-Nicolson and a three-level linearized ones. Both schemes are applied to the discrete version of Cahn-Hilliard equation obtained through the Galerkin approximation in space. We prove that the sequence of solutions of the mixed three level finite difference scheme combined with the Galerkin approximation converges when the time step length and the space approximation error decrease. We also recall the verification of the second order of this scheme and its unconditional stability with respect to the time variable. A comparative scalability analysis of parallel implementations of the schemes is also presented.

**Keywords:** isogeometric analysis · time-integration schemes · tumor simulations · Cahn-Hilliard equations

## 1 Introduction

Cahn-Hilliard equations are widely used to describe the temporal evolution of two phases of a system engaged in the phase transition, like a solidifying liquid. It is a system of equations that can be reduced to one equation that is first order in time and fourth order in space. When using the finite element method this high spatial order requires the use of smooth spatial basis functions, like the ones coming from the isogeometric analysis (IGA). And, in fact, IGA has been successfully applied to the solution of Cahn-Hilliard equations, cf. [1, 2]. On the other hand, Cahn-Hilliard equations has been applied to model the tumor growth as well, cf. [3, 4]. The complexity of such problems is significant because they involve dynamic chemical and biological processes occurring in living tissues with interactions between cellular and vascular levels. The Cahn-Hilliard equations are applied to model interfaces between blood vessels and host tissue. There

ICCS Camera Ready Version 2021
To cite this paper please use the final published version:
DOI: 10.1007/978-3-030-77980-1_14

are already several models of the tumor evolution [5,6] utilizing the isogeometric analysis concept. In this paper we follow on the approach utilizing Cahn-Hilliard equations described in paper [6]. To solve numerically the equations we propose an adaptation of the linearized three-level time integration scheme presented in [7], that on one hand is implicit and on the other hand makes it possible to use a direct solver at every time step. The approach presented in this paper is an alternative to the one described in [2].

## 2 Strong and weak formulations of Cahn-Hilliard equations

This section presents the strong and weak formulations for the Cahn-Hilliard equations, based on [8]. As a strong one we consider the following Cauchy problem: Find $u \in C^1(0,T;C^4(\Omega))$ such that

$$\begin{aligned} u_t = \nabla \cdot \left(B(u)\nabla\left(-\gamma\Delta u + \Psi'(u)\right)\right) \text{ on } \Omega_T = [0,T]\times\Omega \text{ and} \\ u(0,x) = u_0(x) \text{ on } \Omega, \end{aligned} \tag{1}$$

where $\Omega$ is an open subset of $\mathbb{R}^n$, $n = 2,3$ with smooth boundary, $\gamma > 0$ is a positive constant. The scalar field $u$ is the difference of the two fluid phase concentrations. It belongs to $u \in [-1,1]$. The non-negative $B(u) \geq 0$ is the diffusional mobility, and $\Psi(u)$ is the homogeneous free energy. Following [8] we introduce the Ginzburg-Landau free energy

$$\mathcal{E}(u) = \int_\Omega \left(\frac{\gamma}{2}|\nabla u|^2 + \Psi(u)\right) dx, \tag{2}$$

that allows us to monitor the stability of the numerical simulation. Namely, it is supposed to constantly decrease. Let us consider the following boundary conditions

$$\begin{aligned} &u = 0 \text{ in } (0,T)\times\Gamma_D, \quad \tfrac{\partial u}{\partial \mathbf{n}} = 0 \text{ on } \Omega_T, \\ &\mathbf{n}\cdot\left(B(u)\nabla\left(-\gamma\Delta u + \Psi'(u)\right)\right) = 0 \text{ in } (0,T)\times(\partial\Omega\setminus\Gamma_D), \end{aligned} \tag{3}$$

for $\Gamma_D \subset \partial\Omega$ with $\sigma(\Gamma_D) > 0$. Next, following [8], we define

$$\begin{aligned} B(u) &= 1-u^2, \\ \Psi(u) &= \frac{\theta}{2}\left((1+u)\log(1+u) + (1-u)\log(1-u)\right) + 1 - u^2, \end{aligned} \tag{4}$$

where $\theta = 1.5$.

In order to pass to the weak formulation, let us define the following Hilbert space

$$V = \left\{ v \in H^2(\Omega) : \mathbf{tr}(v) = 0 \text{ on } \Gamma_D \text{ and } \frac{\partial u}{\partial \mathbf{n}} = 0 \text{ on } \Omega \right\} \tag{5}$$

ICCS Camera Ready Version 2021
To cite this paper please use the final published version:
DOI: 10.1007/978-3-030-77980-1_14

with the inner product inherited from $H^2(\Omega)$, where **tr** is the $\Gamma_D$-related trace operator on $H^2(\Omega)$. Next, following [1, 8] we introduce the space differential operator $A : H^2(\Omega) \to (H^2(\Omega))'$, such that

$$\begin{aligned} \langle A(u), w\rangle = \int_\Omega (\gamma \Delta u \nabla \cdot (B(u)\nabla w) + (B\Psi'')(u)\nabla u \cdot \nabla w)\, dx, \\ \forall w \in H^2(\Omega). \end{aligned} \tag{6}$$

We also introduce the simple dualizing operator $\tau : H^1(\Omega) \to (H^1(\Omega))'$ such that

$$\langle u, w\rangle = \int_\Omega u \cdot w\, dx, \;\; \forall w \in H^1(\Omega). \tag{7}$$

and the time-derivative operator $\cdot_t : C^1(0,T;H^1(\Omega)) \to C(0,T;(H^1(\Omega))')$

$$\langle u_t(t), w\rangle = \left\langle \frac{\partial u}{\partial t}(t), w \right\rangle, \;\; \forall w \in H^1(\Omega), \forall t \in [0,T]. \tag{8}$$

Then, we are able to introduce the second variational equation preserving the classical, Frechet derivative with respect to the time variable: We seek for $u \in C^1(0,T;V)$ such that

$$\begin{aligned} \langle u_t(t), w\rangle + \langle A(u(t)), w\rangle = 0 \;\; \forall w \in V, \;\; \forall t \in [0,T] \;\text{ and} \\ u(0,x) = u_0(x) \text{ a.e. on } \Omega. \end{aligned} \tag{9}$$

The above weak formulation of Cahn-Hilliard equation with boundary conditions (3) can be rewritten in a brief, dual form

$$u_t(t) + A(u(t)) = 0, \;\; u(0) = u_0. \tag{10}$$

## 3 Semi-discrete Galerkin formulation

Let us introduce the sequence of approximation finite dimensional spaces $\{X_n\}$, such, that $X_{n_1} \subset X_{n_2} \subset V$, $\forall n_2 > n_1$, moreover $\overline{\bigcup_n X_n} = V$ in the strong topology induced from $H^2(\Omega)$. The sequence $\{X_n\}$ can be obtained in particular by using the Finite Element Method for creating the base for the first subspace $X_{n_0}$, and the proper adaptive policy for obtaining the consecutive spaces $X_m, m > n_0$ (see e.g. [9]).

Now, we are able to introduce the sequence of Galerkin problems with a continuous time leading to find $u_n \in C^1(0,T;X_n)$ so, that

$$(u_n)_t(t) + A(u_n(t)) = 0, \;\; u_n(0) = u_0. \tag{11}$$

For the sake of simplicity we assume that $u_0 \in \bigcap_n X_n$. As far as we use the same notation for the time derivative and $A$ operators as in (10), they are now the restrictions of operators used there to the space $C^1(0,T;X_n)$.

ICCS Camera Ready Version 2021
To cite this paper please use the final published version:
DOI: 10.1007/978-3-030-77980-1_14

## 4 Finite difference schemes

In order to solve approximately the semi-discrete Galerkin equation (11) in the particular space $C^1(0,T;X_n)$ we can apply a finite-difference scheme along the time variable $t \in [0,T]$. Because explicit schemes, like Euler, are unstable in the case of Cahn-Hilliard equation, in the sequel we will consider only implicit schemes.

We introduce a mesh in the time domain $S_\tau = \{i\tau; i = 0,\dots,K\} \subset [0,T]$, where $K\tau = T$ and $\tau$ stands for the length of the time step. Let $g \in C(0,T;X_n)$ be an arbitrary function. We will denote by $g_\tau = g|S_\tau$ the restriction of $g$ to the mesh $S_\tau$, so that $g_\tau^i = g(t\tau) \in X_n, i = 0,\dots,K$ and $g_\tau = \{g_\tau^i\} \in (X_n)^{K+1}$.

Let us consider the following Crank-Nicolson integration scheme for the semi-continous variatonal formulations of the Cahn-Hilliard equation (11):

We are looking for $u_{n\tau} : S_\tau \to X_n$ such that

$$\begin{aligned} \left\langle \tfrac{u_{n\tau}^{i+1}-u_{n\tau}^{i}}{\tau}, w \right\rangle + \tfrac{1}{2}\langle A(u_{n\tau}^{i+1}) + A(u_{n\tau}^{i}), w\rangle \;&=\; 0, \\ u_{n\tau}^0 = u_0, \;\; \forall w \in X_n, \;\; i &= 0,\dots,K. \end{aligned} \tag{12}$$

This scheme is unconditionally stable with respect to the time step $\tau$. Unfortunately, the price for this property is very high, because it requires solving nonlinear variational equation at each time step. It is also worth noticing that the Crank-Nicolson scheme can be extended to the so-called generalized $\alpha$-scheme presented in [10], where the time integration step can be adapted.

Let us assume now that we additionally know a solution $u_{(-1)} \in X_n$ to (11) at the time instance $-\tau$. In other words, we have double initial conditions $u_{n\tau}^{-1} = u_{(-1)}, u_{n\tau}^0 = u_0 \in X_n$. We may then define the following three-level linearized integration scheme:

We are looking for $u_{n\tau} : \{-\tau\} \cup S_\tau \to X_n$ such that

$$\begin{aligned} \left\langle \tfrac{u_{n\tau}^{i+2}-u_{n\tau}^{i}}{2\tau}, w \right\rangle + \left\langle \tfrac{1}{2}\, DA|_{u_{n\tau}^{i+1}}\,(u_{n\tau}^{i+2} + u_{n\tau}^{i} - 2u_{n\tau}^{i+1}) + A(u_{n\tau}^{i+1}), w \right\rangle = 0, \\ u_{n\tau}^{-1} = u_{(-1)},\; u_{n\tau}^0 = u_0, \;\; \forall w \in X_n, \;\; i = -1,0,1,\dots,K. \end{aligned} \tag{13}$$

In contrast to the Crank-Nicolson scheme, we can compute the next-step solution $u_{n\tau}^{i+2}$ by solving linear equation, instead of the nonlinear one, which is usually much more cheaper. The double initial conditions does not cause any problem because if the single initial condition $u_{(-1)} \in X_n$ is given, then $u_0 \in X_n$ can be approximated using, e.g., a single step of the Crank-Nicolson scheme (12).

Now, let us denote by $\{\eta_i\}, i = 1,...,n, n < +\infty$ an arbitrary basis in $X_n$ convenient for solving (11). The solution $u_{n\tau}$ of both mixed schemes can be represented as a sequence of real vectors $\{\alpha^j\}$, $j = 1,\dots,K$, so that $\alpha^j \in \mathbb{R}^n, u_{n\tau}^j = \sum_{i=1}^n \alpha_i^j \eta_i$. Moreover, the basis vectors $\eta_i, i = 1,\dots,n$ will be used as test functions $w \in X_n$. The details of solving equations resulting from both schemes can be found in many books and papers (see e.g. [9]).

ICCS Camera Ready Version 2021
To cite this paper please use the final published version:
DOI: 10.1007/978-3-030-77980-1_14

The scheme (13) becomes a sequence of linear systems with the $n \times n$ matrices $(\mathbf{1}+\tau \mathrm{M}^j)$, $j = 1, \ldots, K$, where $\mathbf{1}$ is the Gram matrix and $\mathrm{M}^j$ denotes the matrix associated with the differential $DA|u_{n\tau}^{j-1}$, both computed with respect to the selected basis in $X_n$.

Finally, the simulation of cancer growth by Cahn-Hilliard equation using the proposed three-level linearized scheme will follow the simple algorithm (see Listing 1).

```
1  BEGIN
2  Choose the space X_n ⊂ V and its basis
       {η_i}, i = 1,...,n;
3  Choose the initial time step τ;
4  Compute initial condition u_(-1) ∈ X_n by projecting
       u(0) on X_n;
5  Compute u_0 ∈ X_n from equation (12);
6  FOR j = 1,...,K
7       Compute u_nτ^j ∈ X_n from equation (13);
8  ENDFOR
9  IF the solution is unsatisfactory
10      SWITCH //perform 1, 2, or both
11          (1) Decrease the time step τ;
12          (2) Improve the space X_n according some
                adaptation rule (see [9]);
13      ENDSWITCH
14      GOTO 4;
15 ENDIF
16 END
```

Listing 1: The algorithm implementing three-level finite-difference scheme (13) for Cahn-Hilliard equation.

The linearized three-level scheme can be also reformulated in a way similar to the generalized $\alpha$-scheme [10], so we can adjust the time integration step adaptively. We can utilize either direct or iterative linear solvers for the computations in every time step.

## 5 Mathematical properties of the linearized three level scheme

Two important asymptotic features of the mixed Galerkin/three-level linearized scheme (13) were studied.

**Observation 1** *If both $B$ and $\Psi''$ are positive constants functions ($B \equiv b > 0$ and $\Psi'' \equiv c > 0$), then Problem (11) has the unique solution in $C^1(0, T; X_n)$ for any $u_0$ and $n$ and the sequence of Galerkin solutions to (11) converges to the solution of (10), i.e. $\|u_n - u\|_{C(0,T;L^2(\Omega))}$ for $n \to +\infty$.*

ICCS Camera Ready Version 2021
To cite this paper please use the final published version:
DOI: 10.1007/978-3-030-77980-1_14

The above observation follows immediately from the Observation 4 in Appendix.

**Observation 2** *Let us assume, that the time network is regular, i.e.* $S = \{t_{-1} = -\tau, t_1 = 0, t_2 = \tau, \ldots, t_{K\tau} = K\tau = T\}$ *and we know* $u(-\tau)$ *and* $u(0) = u_0$ *being the values of the exact solution to (10) for all* $\tau$; $T_l > \tau > 0$, *for some positive constant* $T_l > 0$. *If moreover the assumptions of Observation 1 hold, then:*

1. *Three-level linearized scheme (13) applied for the semi-discrete Galerkin formulation of the Cahn-Hilliard equation (11) has the unique solution* $u^i_{n\tau}$ *for each time step* $i = -1, 0, 1, \ldots, K$.
2. *The sequence of solutions* $\{u_{n\tau}\}$ *to the mixed Galerkin/three-level linearized scheme of solving Cahn-Hilliard equation converges to the solution* $u$ *of the exact variational formulation (10), i.e.*

$$\lim_{n\to+\infty,\tau\to 0} \|u_{n\tau} - u\|_\tau = 0,$$

*where* $\|u\|_\tau = \max\{\|u(i\tau)\|_{L^2(\Omega)}, i = 1, 2, \ldots, K\}$.

The above observation is the simple issue of the Observation 5 in Appendix.

It is worth to notice, that the three-level linearized scheme (13) is unconditionally stable with respect to the time step $\tau$, because its convergence was proven without any assumed dependencies between the time and space (Galerkin) approximations.

Moreover, it can be proven, that the three-level linearized scheme (13) applied for the approximate, semi-discrete (11) variational formulations of Cahn-Hilliard equations is of the second order with respect to the time step $\tau$ (see [11]).

## 6 Scalability analysis

Most approaches to the Cahn-Hilliard equation, including Crank-Nicolson integration schemes (12), result in a sequence of nonlinear algebraic systems. The presented linearized three-level scheme results in a sequence of linear systems, thus its dominating part of computational cost at each time step (namely multifrontal solver applied for solving the linear system) is comparable to the cost of solving a linear variational elliptic problem with a linear operator. Paper [5] describes such a particular case using a $L^2$-projection scheme. Both cases ($L^2$ projection equation for elliptic problem and one step linearized three level scheme for Cahn-Hilliard) possess exactly the same matrix size and structure, thus the same computational cost. All computations for both cases presented in this paper were performed with IGA-FEM [12], which utilizes B-Spline basis functions for the approximation in space domain.

The first goal we try to obtain by numerical experiments is the analysis of software scalability obtained by implementing both schemes (12) and (13). To analyze scalability of the entire scheme it is enough to analyze scalability in a single step, because in each step the most expensive part (i.e., the multifrontal

ICCS Camera Ready Version 2021
To cite this paper please use the final published version:
DOI: 10.1007/978-3-030-77980-1_14

solver execution) is repeated in the same manner and possess almost identical computational cost. In case of scaling Crank-Nicolson scheme computation, only one Newton iteration of solving nonlinear algebraic system was included. The experiment observes the course of computational time regression with respect to increasing processor count.

In order to make computations more convenient in PetIGA interface, each of variational equations (12) and (13) was reformulated to equivalent form: from the single fourth order PDEs (or $H^2$ weak formulation) down to the system of two second order PDEs (or a system of two $H^1$ weak problems).

The computations were performed on a distributed-memory Linux cluster. One processor per node is utilized, up to 256 STAMPEDE Linux cluster nodes. The PETSC interface [13–15] delivers multiple solvers including MUMPS [16–18], SuperLU [19, 20] and PaSTiX [21]. All of benchmarks presented in this paper were performed on a $L^2$ projection problem coded in PetIGA [22] interface (an IGA-FEM overlay to PETSC). The interface and solvers control execution in concurrent environment. The aim was to examine and compare scalability and computational cost of different combinations of schemes and solvers (implementations).

Tests were executed for the number of processors increasing from 1 to 256. Various types of B-Spline basis functions [12] resulted in various global regularity utilized. Quartics $C^3$ used for the first formulation are compared with quadratics $C^0$ used for the second formulation, over the mesh with $128 \times 128$ elements, see Figure 1. Octics $C^7$ used for the first formulation are compared with quartics $C^0$ used for the second formulation, over the mesh with $256 \times 256$ elements, see Figure 2. It can be noted that for both cases, the MUMPS solver for the second formulation (for $C^0$ basis) outperforms all the other solvers with increased number of processors.

Preliminary results are presented in Figure 3. The software implementing three-level linearized scheme scales in the same manner as Crank-Nicolson for all tested multi-frontal solvers. Moreover it can be noted that higher continuity B-Spline basis functions tend to compute faster for the same mesh sizes.

The second goal of numerical experiments is to compare both schemes by simulating benchmarks of single tumor growth. Both simulations performed for 8000 time steps present similar final images of tumor cell concentration. It can be concluded that utilizing three-level linearized time integration scheme doesn't degrade the accuracy in comparison with state-of-the-art Crank-Nicolson time integration scheme.

## 7 Conclusions

The theoretical results presented in this paper complete the formal analysis of the mixed three-level linearized finite-difference-Galerkin numerical scheme applied for solving the Cahn-Hiliard equation. We have obtained theorems guaranteeing the existence and the uniqueness of solutions to the exact continuous/variational problem (8), (10) and its semi-discrete Galerkin version (11). We have

ICCS Camera Ready Version 2021
To cite this paper please use the final published version:
DOI: 10.1007/978-3-030-77980-1_14

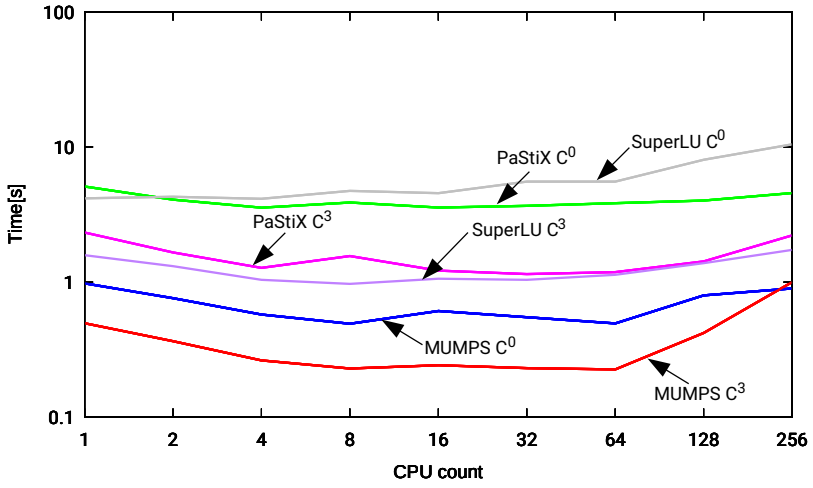


Fig. 1: Comparison of scalability for quartics $C^3$ used for the first formulation with quadratics $C^0$ used for the second formulation, over the mesh with $128 \times 128$ elements.

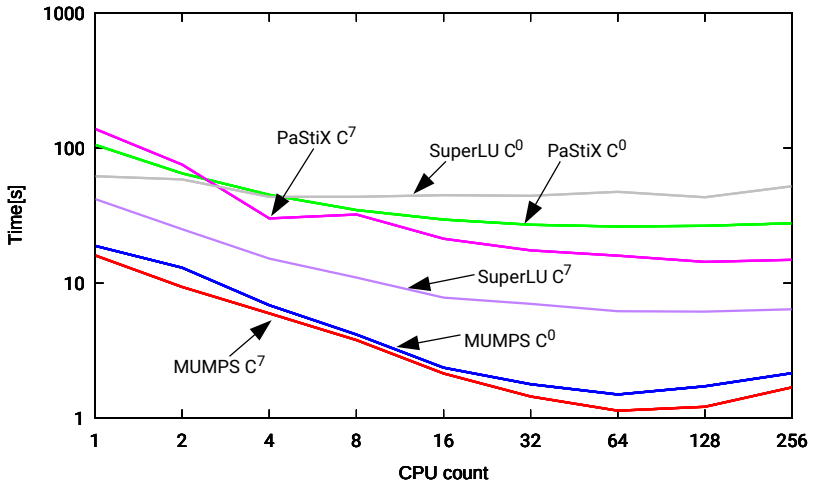


Fig. 2: Comparison of scalability for octics $C^7$ used for the first formulation with quartics $C^0$ used for the second formulation, over the mesh with $256 \times 256$ elements.

ICCS Camera Ready Version 2021
To cite this paper please use the final published version:
DOI: 10.1007/978-3-030-77980-1_14

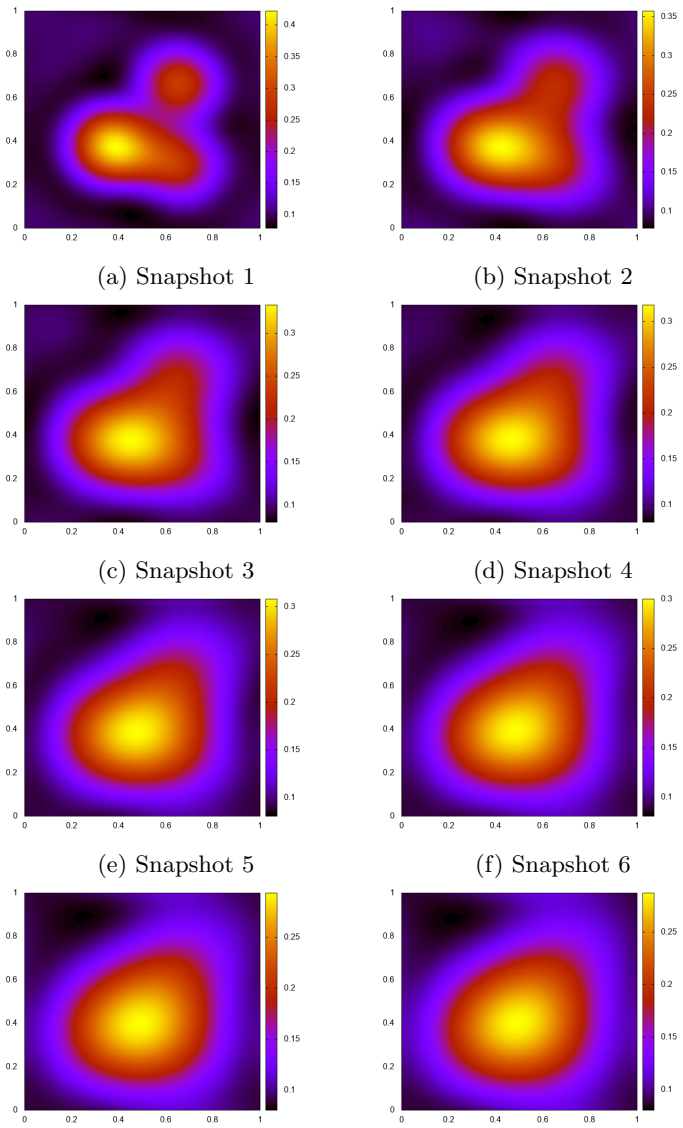

(a) Snapshot 1 (b) Snapshot 2

(c) Snapshot 3 (d) Snapshot 4

(e) Snapshot 5 (f) Snapshot 6

(g) Snapshot 7 (h) Snapshot 8

Fig. 3: Snapshots from the tumor growth simulations with the Cahn-Hilliard equation.

ICCS Camera Ready Version 2021
To cite this paper please use the final published version:
DOI: 10.1007/978-3-030-77980-1_14

also shown the convergence of the solutions of (11) to the exact solution when the Galerkin approximation error decays. Next, we have proved the convergence of the solutions of three-level linearized scheme (13) when both space and time approximations are improved ($n \to \infty$, $\tau \to 0$) and that the scheme is unconditionally stable with respect to the time variable. Additionally, we refer to the proof of the second order of (13) with respect to the time variable.

The scheme is flexible to incorporate different linear solvers and well dedicated to particular B-Spline basis functions. The software implementing three-level linearized scheme scales in the same manner as Crank-Nicolson for all tested multi-frontal solvers. Moreover it can be noted that higher continuity B-Spline basis functions tend to compute faster for the same mesh sizes. It can be also observed, that for both cases, the MUMPS solver for the second formulation (for $C^0$ basis) outperforms all the other solvers with increased number of processors.

Both, theoretical and experimental results presented in this paper show, that the proposed three level linearized time integration scheme is an advantageous tool for solving initial boundary value problems for Cahn-Hiliard equations. Theorems and observations proved that the scheme is as well conditioned as Crank-Nicolson one, concerning convergence, stability and order. Numerical results show that utilizing three-level linearized time integration scheme doesn't degrade the accuracy in comparison with state-of-the-art time integration scheme - Crank-Nicolson one.

The main advantage of the three-level integration scheme over Crank-Nicolson is lower computational cost. It always requires only one linear system to be solved within each time step. In case of non-linear Cahn-Hiliard equation Crank-Nicolson scheme (12) may require solving multiple linear system within each time step.

The effective numerical model of the Cahn-Hiliard equation is crucial for simulating tumor growth abd then is helpful by the medical diagnosis and therapy of this group of heavy diseases.

The future work may involve incorporating the Cahn-Hilliard based models with supermodeling approach [23–25].

## Acknowledgement

The Authors are thankful for support from the funds assigned to AGH University of Science and Technology by the Polish Ministry of Science and Higher Education.

## Appendix: Convergence of the mixed 3-level linearized scheme

In this section we prove the convergence of the 3-level scheme (13) . Crucial properties of operator $A$ are its continuity and coercivity, which are used to prove the convergence of the numerical schema. They are formulated in the

ICCS Camera Ready Version 2021
To cite this paper please use the final published version:
DOI: 10.1007/978-3-030-77980-1_14

following way: there exist positive constants $m$ and $M$ and function $\zeta$ satisfying $\zeta(s) \to +\infty (s \to +\infty)$ such that for every $u, v \in V$ we have

$$\|A(u) - A(v)\|_{V'} \leq M\|u - v\|_V \tag{14a}$$
$$\langle A(u) - A(v), u - v\rangle_{V'\times V} \geq m\|u - v\|_V^2 \tag{14b}$$
$$\langle A(u), u\rangle_{V'\times V} \geq \zeta(\|u\|_V)\ \|u\|_V \tag{14c}$$

A sample case when the above conditions hold is shown in the following observation.

**Observation 3** *Assume that both $B$ and $\Psi''$ are positive constants ($B \equiv b > 0$ and $\Psi'' \equiv c > 0$). Then, conditions (14) hold.*

*Proof.* This is in fact a linear case, i.e.

$$\langle A(u), w\rangle = \int_\Omega (\gamma b \Delta u \Delta w + bc\nabla u \nabla w)\, dx.$$

Therefore,

$$|\langle A(u), w\rangle| \leq \gamma b\|\Delta u\|_{L^2(\Omega)}\|\Delta w\|_{L^2(\Omega)} + bc\|\nabla u\|_{L^2(\Omega;\mathbb{R}^n)}\|\nabla w\|_{L^2(\Omega;\mathbb{R}^n)},$$

which yields (14a) with, e.g., $M = b(\gamma + c)$. Moreover,

$$\begin{aligned}\langle A(u), u\rangle &= \int_\Omega \left(\gamma b(\Delta u)^2 + bc|\nabla u|^2\right) dx \\ &= \gamma b\|\Delta u\|^2_{L^2(\Omega)} + bc\|\nabla u\|^2_{L^2(\Omega;\mathbb{R}^n)},\end{aligned}$$

which, together with an appropriate version of Poincaré inequality, gives us (14c). Finally, in this case, it is easy to see that (14b) is a consequence of (14c).

Let assume now, that we know the solution to (10) in some interval $[-T_l, 0]$ for $T_l > 0$. We can introduce the time grids

$$S_\tau = \{i\tau;\ i = 1, 2, \ldots, K;\ \tau < t_0,\ K\tau = T\}. \tag{15}$$

The arbitrary function $g : [-T_l, T] \to X_n((X_n)')$ can be restricted to $S_\tau$, then we obtain the grid function $g_\tau = \{g_\tau^{-1} = g(-\tau), g_\tau^0 = g(0), g_\tau^1 = g(\tau), g_\tau^2 = g(2\tau), \ldots, g_\tau^K = g(K\tau)\}$.

Let us denote by $V_n$ and $V_n'$ the vector spaces being the the restrictions of $C(-T_l, T; X_n)$ and $C(-T_l, T; X_n')$ to the network $S_\tau$ equipped with the norms:

$$\begin{aligned}\|g_\tau\|_{K\tau} &= \max\{\left\|g_\tau^i\right\|_{H^2(\Omega)}, i = -1, 0, 1, 2, \ldots, K\}, \\ \|g_\tau\|'_{K\tau} &= \max\{\left\|g_\tau^i\right\|_{H^{-2}(\Omega)}, i = -1, 0, 1, 2, \ldots, K\},\end{aligned} \tag{16}$$

respectively.

ICCS Camera Ready Version 2021
To cite this paper please use the final published version:
DOI: 10.1007/978-3-030-77980-1_14

We are ready now to define the time grid operator $R_\tau : V_n \to V_n'$ as the collection of coordinate operators

$$(R_\tau(g_\tau))^i = \frac{g_\tau^{i+1} - g_\tau^i}{2\tau} + A(g_\tau^i) + \frac{1}{2} DA|_{g_\tau^{i+1}}(g_\tau^{i+2} - 2g_\tau^i + g_\tau^{i-1}) \qquad (17)$$

associated with the three-level linearized scheme (13). The mixed Galerkin three-level linearized scheme discrete problem can be formulated as follows:
Let us assume, that the exact solution $u$ of (10) is well-known and continuous with respect to the time variable on the interval $[-T_l, 0]$ and moreover $\forall t \in [-T_l, 0]$ $u(t) \in \bigcap_n X_n$. We are looking for $u_{n\tau} \in V_n$ that satisfies

$$R_\tau(u_{n\tau}) = 0 \quad \text{and} \quad u_{n\tau}^{-1} = u(-\tau),\ u_{n\tau}^0 = u_0. \qquad (18)$$

Notice, that for the sake of simplicity the notation of the operator $R_\tau$ is polymorphic in the same way as the notation of $A$ here, i.e. denote the families of operators for all $n$.

Solving nonlinear parabolic variational equations of type (10) by using mixed Galerkin 3-leveled linearized schema was intensively studied in papers [26, 27]. Observation 3 states the fact that operator $A$ satisfies the assumptions of Theorems 1 and 2 from paper [27]. In particular, Theorem 1 in [27] implies that:

**Observation 4** *Under the assumptions of Observation 3 the following statements hold:*

1. *Problem (10) has the unique solution in* $L^2(0,T;V) \cap C(0,T;L^2(\Omega))$ *for any* $u_0$.
2. *Problem (11) has the unique solution in* $C^1(0,T;X_n)$ *for any* $u_0$ *and* $n$.
3. $\|u_n - u\|_{C(0,T;L^2(\Omega))}$ *for* $n \to +\infty$.

Moreover, taking into account Theorem 2 in [27] we have:

**Observation 5** *The problem (18) has the unique solution for any* $u(-\tau)$ *and* $u_0$*, moreover*

$$\lim_{n\to+\infty,\tau\to 0} \|u_{n\tau} - u\|_\tau = 0$$

*where* $\|u\|_\tau = \max\{\|u(i\tau)\|_{L^2(\Omega)}, i = 1, 2, \ldots, K\}$.

## References

1. H. Gómez, V. M. Calo, Y. Bazileves, T.J.R. Hughes, *Isogeometric analysis of the Cahn-Hilliard phase-field model*, Computer Methods in Applied Mechanics and Engineering, 197 (2008) 4333-4352.

ICCS Camera Ready Version 2021
To cite this paper please use the final published version:
DOI: 10.1007/978-3-030-77980-1_14

2. H. Gómez, T.J.R. Hughes, *Provably unconditionally stable, second-order time-accurate, mixed variational methods for phase-field models*, Journal of Computational Physics, 230 (2011) 5310-5327.
3. A. Hawkins-Daarud, S. Prudhomme, K. van der Zee, J. T. Oden, *Bayesian calibration, validation, and uncertainty quantification of diffuse interface models of tumor growth*, Journal of Mathematical Biology, 67(6-7) (2013) 1457-1485.
4. X. Wu, G. J. van Zwieten, K. van der Zee, *Stabilized second-order convex splitting schemes for Cahn–Hilliard models with application to diffuse-interface tumor-growth models*, Numerical Methods in Biomechanical Engineering, 30(3) (2014), 180–203.
5. M. Łoś, A. Kłusek, M. A. Hassaan, K. Pingali, W. Dzwinel, M. Paszyński, *Parallel fast isogeometric L2 projection solver with GALOIS system for 3D tumor growth simulations*, Computer Methods in Applied Mechanics and Engineering, 343, (2019) 1-22
6. V. Puzyrev, M. Łoś, G. Gurgul, V. M. Calo, W. Dzwinel, M. Paszyński, *Parallel splitting solvers for the isogeometric analysis of the Cahn-Hilliard equation*, Computer Methods in Biomechanics and Biomedical Engineering 22(16) (2019) 1269-1281.
7. M. Woźniak, M. Smołka, A. Cortes, M. Paszyński, R. Schaefer, *Scalability of Direct Solver for Non-stationary Cahn-hilliard Simulations with Linearized Time Integration Scheme*, Procedia Computer Science, 80 (2016) 834-844.
8. C. M. Elliott, H. Garcke, *On the Cahn-Hilliard equation with degenerate mobility* SIAM Journal of Mathematical Analysis, 27 (1996) 404-423.
9. Demkowicz, L. and Kurtz, J. and Pardo, D. and Paszyński, M. and Rachowicz, W. and Zdunek, A., Computing with hp Finite Elements. II. Frontiers: Three-Dimensional Elliptic and Maxwell Problems with Applications, Chapman & Hall/CRC, 2007.
10. Jansen, K.E. and Whiting, C.H. and Hulbert, G.M. *A generalized-$\alpha$ method for integrating the filtered Navier-Stokes equations with a stabilized finite element method*, Computer Methods in Applied Mechanics and Engineering, 190 (2000) 305-319.
11. M. Woźniak, M. Smołka, A. Cortes, M. Paszyński and R. Schaefer, *Scalability of direct solver for non-stationary Cahn-Hilliard simulations with linearized time integration scheme*, Procedia Computer Science, 80 (2016) 834-844.
12. J. Austin Cottrell, Thomas J. R. Hughes, and Yuri Bazilevs., *Isogeometric Analysis: Toward Integration of CAD and FEA*, John Wiley & Sons, Ltd., August 2009.
13. S. Balay, S. Abhyankar, M. F. Adams, J. Brown, P. Brune, K. Buschelman, V. Eijkhout, W. D. Gropp, D. Kaushik, M. G. Knepley, L. Curfman McInnes, K. Rupp, B. F. Smith, H. Zhang, *PETSc Web Page*, *http://www.mcs.anl.gov/petsc* (2014)
14. S. Balay, S. Abhyankar, M. F. Adams, J. Brown, P. Brune, K. Buschelman, V. Eijkhout, W. D. Gropp, D. Kaushik, M. G. Knepley, L. Curfman McInnes, K. Rupp, B. F. Smith, H. Zhang, *PETSc User Manual*, Argonne National Laboratory ANL-95/11 - Revision 3.4 (2013)
15. S. Balay, W. D. Gropp, L. Curfman McInnes, B. F. Smith, *Efficient Management of Parallelism in Object Oriented Numerical Software Libraries*, Modern Software Tools in Scientific Computing, Editors E. Arge, A. M. Bruaset and H. P. Langtangen (1997) Birkhä user Press.
16. P. R. Amestoy , I. S. Duff, *Multifrontal parallel distributed symmetric and unsymmetric solvers*, Computer Methods in Applied Mechanics and Engineering, 184 (2000) 501-520.


ICCS Camera Ready Version 2021
To cite this paper please use the final published version:
DOI: 10.1007/978-3-030-77980-1_14

17. P. R. Amestoy, I. S. Duff, J. Koster, J.Y. L'Excellent, *A fully asynchronous multifrontal solver using distributed dynamic scheduling*, SIAM Journal of Matrix Analysis and Applications, 1(23) (2001) 15-41.
18. P. R. Amestoy, A. Guermouche, J.-Y. L'Excellent, S. Pralet, *Hybrid scheduling for the parallel solution of linear systems*, Computer Methods in Applied Mechanics and Engineering, 2(32) (2001) 136-156.
19. Xiaoye S. Li, *An Overview of SuperLU: Algorithms, Implementation, and User Interface*, TOMS Transactions on Mathematical Software, 31(3) (2005) 302-325.
20. X.S. Li, J.W. Demmel, J.R. Gilbert, iL. Grigori, M. Shao, I. Yamazaki, *SuperLU Users' Guide*, Lawrence Berkeley National Laboratory, LBNL-44289 *http://crd.lbl.gov/ xiaoye/SuperLU/* (1999).
21. P. Hénon, P. Ramet, J. Roman, *PaStiX: A High-Performance Parallel Direct Solver for Sparse Symmetric Definite Systems*, Parallel Computing, 28(2) (2002) 301-321.
22. N. Collier, L. Dalcin, V. M. Calo., *PetIGA: High-performance isogeometric analysis*, arxiv, (1305.4452), (2013) http://arxiv.org/abs/1305.4452
23. W. Dzwinel, A. Kłusek and M. Paszyński, *A concept of a prognostic system for personalized anti-tumor therapy based on supermodeling*, Procedia Computer Science, 108C (2017) 1832–1841
24. W. Dzwinel, A. Kłusek, O. V. Vasilyev, *Supermodeling in simulation of melanoma progression*, Procedia Computer Science, 80 (2016) 999-1010.
25. L. Siwik, M. Łoś, A. Kłusek, W. Dzwinel, M. Paszyński, K. Pingali, *Supermodeling of tumor dynamics with parallel isogeometric analysis solver*, arXiv:1912.12836
26. Schaefer R., Sędziwy S., *Filtration in cohesive soils. Part II - Numerical approach*, Computer Assisted Mechanics and Engineering Sciences (CAMES), Vol. 6, 1999, pp. 15-26,
27. Schaefer R., Sędziwy S., *Filtration in cohesive soils. Part I - The mathematical model*, Computer Assisted Mechanics and Engineering Sciences (CAMES), Vol. 6, 1999, pp. 1-13.

ICCS Camera Ready Version 2021
To cite this paper please use the final published version:
DOI: 10.1007/978-3-030-77980-1_14